# SOLITON SPECTRA OF RANDOM WATER WAVES IN SHALLOW BASINS

J.-P. Giovanangeli[1], C. Kharif[1] and Y.A. Stepanyants[2,3,*]

**Abstract.** Interpretation of random wave field on a shallow water in terms of Fourier spectra is not adequate, when wave amplitudes are not infinitesimally small. A nonlinearity of wave fields leads to the harmonic interactions and random variation of Fourier spectra. As has been shown by Osborne and his co-authors, a more adequate analysis can be performed in terms of nonlinear modes representing cnoidal waves; a spectrum of such modes remains unchanged even in the process of nonlinear mode interactions. Here we show that there is an alternative and more simple analysis of random wave fields on shallow water, which can be presented in terms of interacting Korteweg–de Vries solitons. The data processing of random wave field is developed on the basis of inverse scattering method. The soliton component obscured in a random wave field is determined and a corresponding distribution function of number of solitons on their amplitudes is constructed. The approach developed is illustrated by means of artificially generated quasi-random wave field and applied to the real data interpretation of wind waves generated in the laboratory wind tank.

**Mathematics Subject Classification.** 76B15, 76B25, 35Q51, 35Q53, 37K40

## 1. Introduction

The traditional approach in the problem of wind wave study is based on the analysis of Fourier spectra and determination of their peculiarities. There is a vast number of papers both theoretical and experimental where this problem has been considered; it is impossible to list all of them here. Therefore, we refer only to the review chapter "Wind waves" by Zaslavsky and Monin in the book [14] where a reader can find key references in this field. A lot of interesting and useful information has been obtained about wind waves, and their analysis and interpretation have been implemented in terms of Fourier spectra.

Meanwhile, the Fourier analysis of wind waves provides researchers with only some piece of objective information whereas many important features of wind waves remain hidden. One of the serious obstacles making the Fourier analysis ineffective in application to surface oceanic waves is the nonlinear character of such waves, whereas the Fourier analysis is a linear operation applicable to systems obeying the superposition principle.

[1] Aix Marseille Université, CNRS, Centrale Marseille, IRPHE UMR 7342, 13384 Marseille, France.

[2] Faculty of Health, Engineering and Sciences, University of Southern Queensland, Toowoomba, QLD 4350, Australia.

[3] Department of Applied Mathematics, Nizhny Novgorod State Technical University n.a. R.E. Alekseev, Nizhny Novgorod 603950, Russia.

* Corresponding author: yuas50@gmail.com

Osborne with co-authors (see, *e.g.*, [20–23, 27] and references therein) have developed the method of non-linear spectral analysis of shallow water waves described by the Korteweg–de Vries (KdV) equation. Osborne's approach is based on the application of the inverse scattering method (ISM) to the analysis of random field data in a one-dimensional space domain with the periodic boundary conditions. The main idea of his approach was in the presentation of complex initial disturbance in terms of a set of elliptic functions (cnoidal waves). These functions can be considered as the nonlinear eigenmodes which are preserved in the process of wave field evolution in contrast to the linear sinusoidal eigenmodes. This means that a nonlinear wave spectrum calculated on the basis of these modes is invariant in time while a usual Fourier spectrum is variable due to nonlinear interactions between the different sinusoidal harmonics. An important feature of nonlinear eigenmodes is their reducibility to the sinusoidal eigenmodes in the case of small amplitudes. In other words, a nonlinear spectrum naturally reduces to the Fourier spectrum if the analyzed wave field is quasi-linear. However, the mathematical and numerical machinery used for calculation of nonlinear eigenmodes is not simple in contrast to the linear case and, apparently, it is impractical especially for the applied mariner engineers.

Here we propose a very similar to Osborne's, but a bit different approach to the analysis of random water waves that is also based on the application of ISM. The essential feature of our approach is the interpretation of a random initial wave field in terms of an ensemble of solitons and quasi-linear ripples rather than the set of elliptic eigenmodes (a similar approach was recently realised in Ref. [5]). The idea is illustrated by an example of shallow water waves described by the classical KdV equation with the random initial data. If one takes some portion of random field data (which should be long enough), the number of solitons, their amplitudes, speeds, characteristic durations, etc., can be calculated then by means of ISM (*e.g.*, by solving numerically the associated Sturm–Louiville problem) or by the direct numerical simulation of the corresponding KdV equation. In both cases, the numerical codes are currently very well developed and easily available. In the meantime, the knowledge of number of solitons obscured in the random wave field, their parameters and statistics is a matter of independent interest per se. We describe our approach below in detail and give some examples (preliminary results were reported at the conference OCEANS'13 MTS/IEEE in San Diego, USA [11]).

Before we start, it is useful to remind that the soliton turbulence of rarified soliton ensembles in strongly integrable systems is trivial to certain extent – the distribution function of solitons is unchanged in time [30, 31] (the definition of strongly and weakly integrable systems is given in [31]). This is a consequence of trivial character of soliton interactions in such systems. The solitons do not change their parameters after collisions, and only the paired collisions occur between them. However, the dynamics of a dense ensemble of solitons is more complicated and soliton turbulence is nontrivial even in the integrable nonlinear wave equations [7–9]. In particular, in reference [8] the quantitative criterion of the term "dense soliton gas" was introduced and was shown that the density of KdV soliton gas is bounded from above. The critical gas density, apparently, depends on soliton distribution function, which makes important the determination of such function in a concrete physical problem such as water wave turbulence. Numerical experiments confirming the developed theory in reference [8] for the particular model distribution functions were reported in [3].

The KdV model considered here is the typical example of strongly integrable system applicable to real physical systems. This makes topical the development of handy methods of extraction of soliton distribution function from natural complex fields. One of the experimental approaches to the solution of this practical problem has been considered for internal waves in Okhotsk Sea [19] and another example of processing of surface wave observational data was reported in reference [5]. We hope, this publication will stimulate further interest to this important problem.

## 2. The Korteweg–de Vries model and data processing

Let us assume that there is a data of recorded surface waves at some fixed point $x_0$ of a shallow-water basin. So that the elevation $\eta$ of the water level at this point is the known function of time: $\eta(x_0, t) = f(t)$ where $f(t)$ is some random function. A typical example of random surface waves usually measured in shallow-water basin is shown in Figure 1. Here these data were artificially produced by means of a computer using the random number generator just to illustrate the idea of our approach.
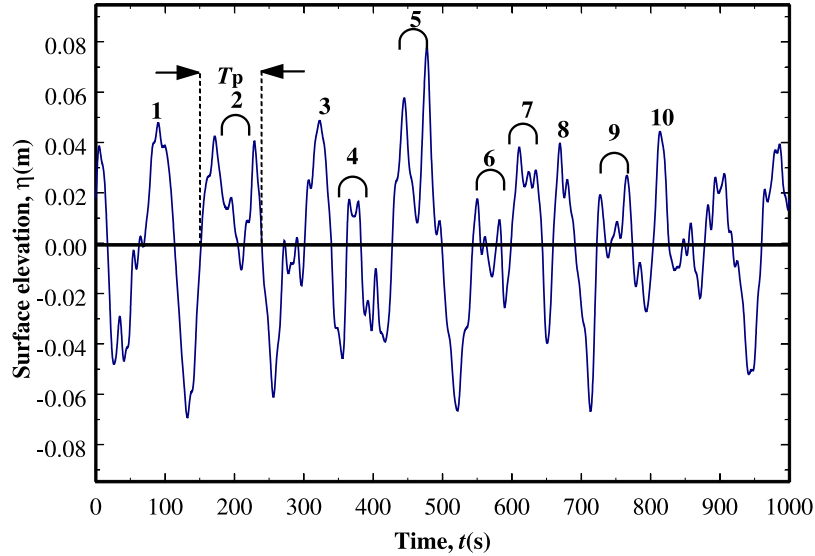
FIGURE 1. A typical example of random surface waves in a shallow water basin.

For the description of further space evolution of data measured at the point $x_0$, the so-called, timelike KdV (TKdV) equation [23] is used:

$$\frac{\partial \eta}{\partial x} + \frac{1}{c_0}\frac{\partial \eta}{\partial t} - \alpha\eta\frac{\partial \eta}{\partial t} - \beta\frac{\partial^3 \eta}{\partial t^3} = 0, \tag{2.1}$$

where $c_0 = \sqrt{gh}; \alpha = 3/(2c_0 h); \beta = h^2/(6c_0^3)$ with $g$ being the acceleration due to gravity and $h$ being an unperturbed water depth.

In the process of evolution of an initial perturbation one can expect emergence of a number of solitons with different amplitudes and phases (*e.g.*, time markers of soliton maxima in the wave record at a given point of observation). Soliton solution to the TKdV equation (2.1) has the form:

$$\eta(x, t) = A\operatorname{sech}^2\frac{t - x/V}{T}, \tag{2.2}$$

where the velocity $V$ and duration $T$ are relate to the amplitude $A$:

$$V = \frac{c_0}{1 - c_0\alpha A/3} \approx c_0\left(1 + \frac{c_0\alpha A}{3}\right), \quad T = \sqrt{\frac{12\beta}{\alpha A}}, \tag{2.3}$$

the approximate formula is valid for small amplitude solitons when $c_0\alpha A/3 \ll 1$.

As it was mentioned in [23], "it may not be possible to observe solitons in real space" because of numerous nonlinear interactions of solitons both with each other and with chaotic radiation background component. However, "it would be naive to conclude that solitons are not present or that their dynamics are not important" in the evolution of the initial perturbation. Inasmuch as solitons are very stable with respect to interaction with others wave perturbations and influence of external effects (such as viscosity, inhomogeneity, etc.), it is a matter of interest to extract them from the irregular components of a wave field and to describe their statistical properties and contribution to the total wave energy.

The solution of this problem can be done by the following way. Let us consider a very long portion of recorded measurement data of surface perturbation at any given point $x_0$. The characteristic duration of this portion $T_p$ is assumed to be much greater than the typical soliton time scale $T$. Let us represent a perturbation with the help of some dimensionless function $\varphi(t)$:

$$\eta(0,t) = U\varphi(t/T_p), \tag{2.4}$$

where $U$ is the characteristic wave "amplitude", *e.g.*, the maximum value of perturbation $\eta(0,t)$ in the considered portion of data.

By means of the transformation

$$u = \frac{\eta}{U}, \quad \xi = -\frac{\alpha U}{T_p}x, \quad \tau = \frac{1}{T_p}\left(t - \frac{x}{c_0}\right). \tag{2.5}$$

Equation (2.1) and the corresponding "initial" perturbation (2.4) can be reduced to the standard form [15] (the term "initial" used here as it is traditionally used in mathematics for the solution of Cauchy problem of differential equations, but in fact, the perturbation is given at the fixed spatial point, *i.e.*, it is rather the boundary condition):

$$u_\xi + uu_\tau + \frac{1}{\sigma^2}u_{\tau\tau\tau} = 0 \tag{2.6}$$

$$u(0,\tau) = \varphi(\tau) \tag{2.7}$$

with one dimensionless parameter $\sigma^2$ known in the oceanography as the Ursell parameter and defined as

$$\sigma^2 = \frac{\alpha U T_p^2}{\beta}. \tag{2.8}$$

As it was mentioned above, we consider the case when the duration of the perturbation is long enough, so that $\sigma^2 \gg 1$. In this case the number of solitons obscured in the "initial" perturbation is also very big in general, and it is reasonable to describe them by the distribution function $f(A)$. This function determines the number of solitons $dN$ within the interval $(A, A + dA)$ [15]

$$\mathrm{d}N = f(A)\mathrm{d}A. \tag{2.9}$$

According to the theory developed in [15], the distribution function can be calculated at large values of $\sigma$ by means of the formula:

$$f(A) = \frac{\sigma}{4\pi\sqrt{3U}}\int_L \frac{\mathrm{d}\tau}{\sqrt{2U\varphi(\tau) - A}}, \tag{2.10}$$

where the interval of integration $L$ is determined by the condition

$$2U\varphi(\tau) > A. \tag{2.11}$$

As follows from equation (2.10), soliton amplitudes are distributed in the interval [15]

$$0 < A < 2U\max[\varphi(\tau)], \tag{2.12}$$

and their total number can be found from the formula

$$N = \int\limits_0^\infty f(A)\,\mathrm{d}A = \left(\frac{\sigma}{\pi\sqrt{6}}\right) \int\limits_{\varphi(\tau)>0} \sqrt{\varphi(\tau)}\,\mathrm{d}\tau. \tag{2.13}$$

Therefore for large $\sigma$ the total number of solitons is determined only by those intervals of $\tau$-axis where function $\varphi(\tau)$ is nonnegative!

As well known, the KdV equation possesses an infinite number of conserved densities $I_n$ [1, 15, 29]. One of them,

$$I_2 = \int\limits_{-\infty}^{+\infty} \eta^2(x,t)\,\mathrm{d}t, \tag{2.14}$$

is proportional to wave energy and therefore is of a special physical interest. For the sake of simplicity we will call this value simply the "energy".

The fraction of energy of a nonsoliton component of a perturbation to the total energy of "initial" perturbation can be determined by means of formulae (18.27), (18.28) and (19.8) in reference [15]:

$$\frac{I_2^{ns}}{I_2^{tot}} = \frac{\displaystyle\int\limits_{\eta(0,\tau)<0} \eta^2(0,\tau)\,\mathrm{d}\tau}{\displaystyle\int\limits_0^{T_p} \eta^2(0,\tau)\,\mathrm{d}\tau}. \tag{2.15}$$

The total energy of a soliton component in the wave field can be readily calculated, if soliton amplitudes are known:

$$I_2^{sol} = 4\sqrt{\frac{\beta}{3\alpha}} \sum_{k=1}^N A_k^{3/2} = \frac{4h}{3\sqrt{3g}} \sum_{k=1}^N A_k^{3/2}. \tag{2.16}$$

In the last expression the values of coefficients $\alpha$ and $\beta$ for surface water waves were used (see above after Eq. (2.1)).

To illustrate the idea of this approach we consider below several examples of different "initial" perturbations.

## 2.1. Sinusoidal perturbation and its modifications

### 2.1.1. A sinusoidal perturbation

Let us study the KdV equation (2.1) with the periodical conditions in time. Let us set $h = 1\,\mathrm{m}$, then $c_0 = 3.13\,\mathrm{m/s}$, $\alpha = 0.479\,\mathrm{s/m^2}$, $\beta = 0.00543\,\mathrm{s^3/m}$. Assume then that the perturbation has the form

$$\eta(0,t) = A\sin\omega t, \tag{2.17}$$

where $A = 0.01\,\mathrm{m}$, $\omega = 0.0628\,1/\mathrm{s}$.

The value of Ursell parameter for this perturbation is $\sigma^2 = 555 \gg \sigma_s^2$, where $\sigma_s^2 \equiv 12$ is the value of Ursell parameter for a single soliton regardless of its amplitude and duration [15].

Figure 2 shows this sinusoidal initial perturbation and the result of its evolution at the distance $x = 1.1\cdot10^3\,\mathrm{m}$ when it is completely disintegrated into the sequence of solitons. After that moment, solitons begin interact with each other and the wave field looks much more complex. In Figure 2 one can distinguish nine different
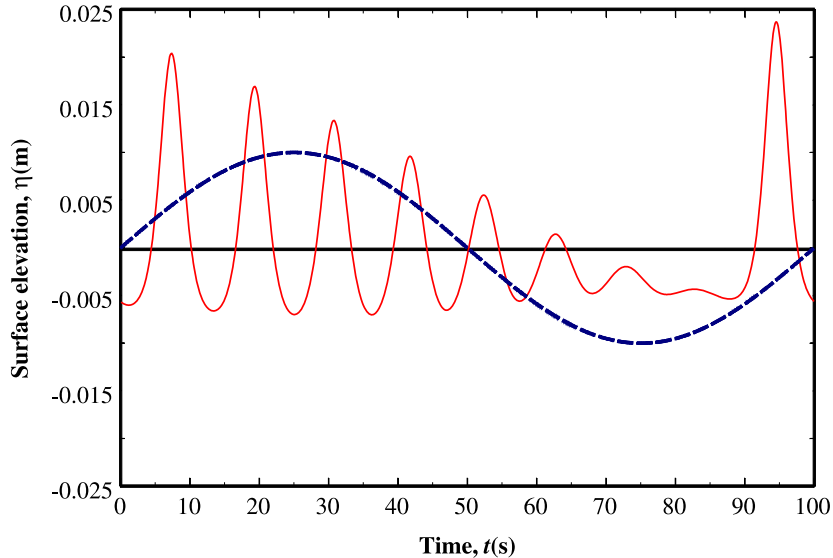
FIGURE 2. Sinusoidal initial perturbation (*dashed line*) and the result of its evolution at the distance $x = 1.1 \cdot 10^4$ m (*solid line*).

TABLE 1. Amplitudes of solitons, $A_k$, emerging from the different initial perturbations. The fifth raw in the Table shows the relative difference $RD$ in the soliton amplitudes of rows three and four in percents, this will be explained in Section 2.1.3.

| Initial pert. | $A_k$ | | | | | | | | |
|---|---|---|---|---|---|---|---|---|---|
| | $A_1$ (mm) | $A_2$ (mm) | $A_3$ (mm) | $A_4$ (mm) | $A_5$ (mm) | $A_6$ (mm) | $A_7$ (mm) | $A_8$ (mm) | $A_9$ (mm) |
| Sin., periodic | 29.39 | 26.7 | 23.72 | 20.37 | 16.38 | 11.61 | 6.625 | 2.876 | 0.792 |
| Sin., pulse | 17.77 | 13.24 | 8.927 | 4.743 | 1.092 | – | – | – | – |
| Half-sin., pulse | 17.71 | 13.24 | 8.863 | 4.738 | 1.171 | – | – | – | – |
| $RD \cdot 100\%$ | 0.34 | 0 | 0.723 | 0.1 | $-6.75$ | – | – | – | – |

solitons whose amplitudes are presented in Table 1. Soliton amplitudes were conditionally defined here as the difference between their maxima and the mean value of two nearest minima.

The total energy of the sinusoidal initial perturbation over a period $T = 2\pi/\omega$ can be easily evaluated

$$I_2^{tot} = \frac{1}{2} \int_0^T \eta^2(0,t) \, dt = \frac{A^2}{2} \int_0^T \sin^2 \omega t \, dt = \frac{A^2 T}{4} = 2.5 \cdot 10^{-3} \, \text{m}^2 \, \text{s}. \tag{2.18}$$

Similarly, the energy of the non-soliton component of the perturbation is (see Eq. (2.15))

$$I_2^{ns} = \int_{\eta(0,\tau)<0} \eta^2(0,\tau) \, d\tau = \frac{A^2}{2} \int_{T/2}^T \sin^2 \omega t \, dt = \frac{A^2 T}{8} = 1.25 \cdot 10^{-3} \, \text{m}^2 \, \text{s}. \tag{2.19}$$
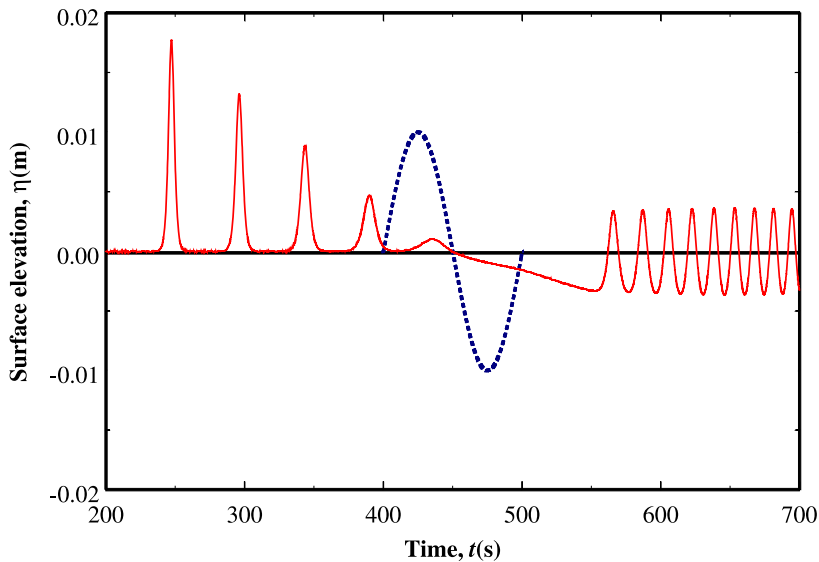
FIGURE 3. A sinusoidal-shape pulse as the initial perturbation (*dashed line*) and the result of its evolution at the distance $x = 6 \cdot 10^4$ m (*solid line*). Only a fragment of a very long quasi-sinusoidal tail behind five solitons is shown in the figure.

Thus, $I_2^{ns} = I_2^{tot}/2$, and the energy of all solitons in this case should be $I_2^{sol} = I_2^{tot}/2 = 1.25 \cdot 10^{-3}$ m$^2$ s. Let us calculate however this energy directly by means of equation (2.16) using data of Table 1 for the soliton amplitudes

$$I_2^{sol} = \frac{4h}{3\sqrt{3}g} \sum_{k=1}^{9} A_k^{3/2} = 4.922 \cdot 10^{-3} \text{ m}^2 \text{ s}. \tag{2.20}$$

This value about four times greater then the expected. The discrepancy can be explained by the incorrect counting of number of solitons, as well as their amplitudes. As has been shown in [24–26], the problem of detection of solitons emerging from the harmonic perturbations is not so simple even within the KdV equation (disintegration of sine wave onto set of solitons was recently studied also within the Gardner equation [16, 17]). Actual number of solitons is always greater then that at the instant of time when they appear from the initial perturbation for the first time in the ordered form. Their amplitudes are also different from those which are seen in Figure 2. We will come back to this issue a bit later, and now let us consider a pulse-type initial perturbations defined on a compact support.

### 2.1.2. A pulse of sinusoidal profile

Consider now a pulse-type initial perturbation having the shape of one period of sine with the same amplitude and characteristic duration as in the previous case (see dashed line in Fig. 3). In the process of evolution this perturbation disintegrates into a sequence of five solitons (see solid line in Fig. 3), whose amplitudes are indicated in the third row of Table 1. An intense oscillatory tail behind the solitons is also appeared; the head portion of this tail is shown in Figure 3.

By comparison of rows two and three of Table 1, one can see that the number of solitons and their amplitudes are absolutely different in the periodic and nonperiodic cases.
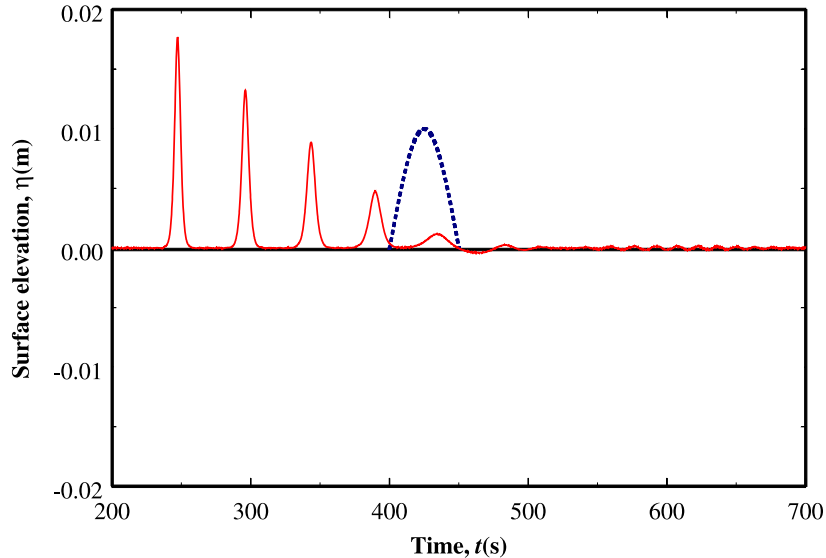
FIGURE 4. A half-sine pulse as the initial perturbation (*dashed line*) and the result of its evolution at the distance $x = 6 \cdot 10^4 \, \mathrm{m}$ (*solid line*).

As all these solitons are practically independent at the distance indicated in Figure 3, their energies can be calculated independently. The calculation of cumulative energy of these five solitons yield:

$$I_2^{sol} = \frac{4h}{3\sqrt{3g}} \sum_{k=1}^{5} A_k^{3/2} = 1.2531 \cdot 10^{-3} \, \mathrm{m^2 \, s}. \tag{2.21}$$

This result already agrees quite well with the theoretical prediction.

### 2.1.3. A half-sine pulse

Let us consider now another pulse-type perturbation which contains only a half period of a sine-function of a positive polarity (see dashed line in Fig. 4).

This perturbation disintegrates into the same number of solitons as in Section 2.1.2. At the same distance $x = 6 \cdot 10^4 \, \mathrm{m}$, the soliton amplitudes are practically the same as in the previous case (*cf.* rows three and four in Tab. 1). The fifth raw in Table 1 shows the relative difference in the soliton amplitudes in percents, $RD = (A_i' - A_i'')/A_i''$, where $A_i'$ and $A_i''$ are the amplitudes of i-th solitons emerged from the sinusoidal and half-sine pulses respectively.

As one can see from Table 1 and Figures 3 and 4, there is no much differences in the corresponding soliton amplitudes for the sinusoidal and half-sine pulses. In the next Subsection we will consider a simple analytical example to justify this numerical observation.

## 2.2. Analytical solutions to the associated Schrödinger equation for the rectangular and meander-type pulses

To understand better the regularity of distribution of amplitudes of solitons emerging from initial perturbations, let us consider two model initial perturbations: the rectangular pulse of positive polarity and amplitude $U_0$ (Fig. 5a) and meander-type pulse whose positive part coincides with the above rectangular pulse and negative
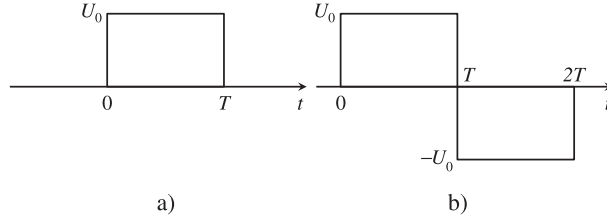
FIGURE 5. Two model initial perturbations: the rectangular pulse (a) and meander-type pulse with the zero mean value (b).

part is the same but of opposite polarity (Fig. 5b). Assume that the duration of positive rectangular pulses are $T$.

According to the ISM [1, 15, 29], to study the evolution of the initial perturbation within the KdV equation (2.1), one have to solve the complementary Schrödinger equation:

$$\psi''(\xi) + \frac{\sigma^2}{6}\left[\varphi(\xi) + E_n\right]\psi(\xi) = 0, \tag{2.22}$$

where $\psi$ is the auxiliary function; $\varphi$ is the dimensionless function describing the shape of the initial perturbation (see above), it has the unit amplitude, i.e., $\varphi_{\max} = 1$, and the unit characteristic duration in the dimensionless variables (2.7). For the case a) in Figure 5, $\varphi = 1$ at $0 \leq \xi \leq 1$ and zero beyond this interval. Similarly, for the case b) in Figure 5, $\varphi = 1$ at $0 \leq \xi \leq 1$, $\varphi = -1$ at $1 < \xi \leq 2$ and zero beyond these intervals. Further, $\sigma^2$ is the Ursell parameter as defined in equation (2.10) with $U \equiv U_0$ and $T_p \equiv T$; $E_n < 0$ with $n = 1, 2, \ldots, N$ are eigenvalues of the Schrödinger equation (2.22). The amplitudes of emerging solitons, $A_n$, are related with the eigenvalues $E_n$ by the simple relation:

$$A_n = -2U_0 E_n. \tag{2.23}$$

The analytical solution to the Schrödinger equation (2.22) with the rectangular potential function can be readily constructed (see e.g., [10, 18]). Omitting simple, but tedious calculations, the result can be presented in the form of two transcendental equations determining eigenvalues $E_n$ of the Schrödinger equation (2.22):

$$\tan\left[\sigma^2\sqrt{\frac{\beta}{24\alpha}(1+E)}\right] = \sqrt{\frac{-E}{1+E}}, \tag{2.24}$$

$$\tan\left[\sigma^2\sqrt{\frac{\beta}{24\alpha}(1+E)}\right] = -\sqrt{\frac{1+E}{-E}}. \tag{2.25}$$

In a similar manner the analytical solution can be found for the initial perturbation shown in Figure 5b. The outcome is presented by the following transcendental equation:

$$\tan\left[\sigma^2\sqrt{\frac{\beta}{6\alpha}(1+E)}\right] = -\frac{\sqrt{1-E^2}\left(\sqrt{-E}+\sqrt{1+E}\right) + \sqrt{1+E}\left[\sqrt{-E(1+E)}+1-E\right]\text{Th}}{\sqrt{1-E^2}\left(\sqrt{-E}-\sqrt{1+E}\right) + \left[\sqrt{-E(1-E)}-\sqrt{1+E}(1+E)\right]\text{Th}}, \tag{2.26}$$
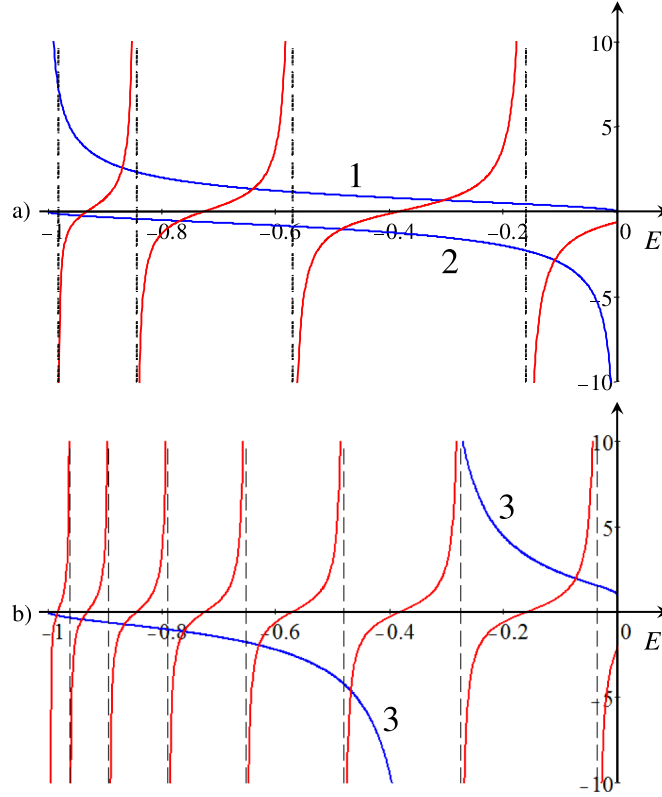
FIGURE 6. (a) Graphical solutions of transcendental equations (2.24) and (2.25). (b) Graphical solutions of transcendental equation (2.26).

where $\mathrm{Th} = \tanh\left(\sigma^2\sqrt{\dfrac{\beta}{6\alpha}(1-E)}\right)$.

Solutions of the transcendental equations (2.24)–(2.26) can be presented graphically as shown in Figures 6a and b, where the series of tan-type curves represent the tangential functions in the left-hand side of these equations, while line 1 represents the right-hand side of equation (2.24), line 2 represents the right-hand side of equation (2.25), and two branches of line 3 represent the right-hand side of equations (2.26).

The plots were generated for the same values of Ursell parameter $\sigma^2 = 555$, the water depth $h = 1\,\mathrm{m}$, and the amplitude of initial perturbations $U_0 = 0.01\,\mathrm{m}$ were chosen the same as in Section 2.1 for the sinusoidal initial functions. In both cases of rectangular and meander-type pulses the number of roots of transcendetal equations (2.24)–(2.26) are the same, $N = 8$. Dashed vertical lines in each figure show positions of several first roots of corresponding equations. The amplitudes of solitons related to these eigenvalues as per equation (2.23) are presented in Table 2.

The last row in the table shows the relative difference in percents between the corresponding soliton amplitudes for the rectangular $A_k^r$ and meander-type $A_k^m$ perturbations: $RD = (A_k^r - A_k^m)/A_k^r$. As one can see from this table, the difference between the corresponding amplitudes $A_k$ is fairly small especially for the first largest solitons, and only for two last solitons of very small amplitudes the difference amounts for about 7% and 31% correspondingly. It can be readily shown that the larger the Ursell parameter, the greater the number of emerging solitons and the smaller the difference in theirs amplitudes.

Thus, one can conclude that the asymptotic theory developed in [15] can provide a good basis for the calculation of statistical properties of solitons obscured in the random wave field. Apparently, the most energetic

TABLE 2. Amplitudes of solitons emerging from the rectangular and meander-type initial perturbations shown in Figure 5.

| Initial pert. | $A_k$ | | | | | | | |
|---|---|---|---|---|---|---|---|---|
| | $A_1$ (mm) | $A_2$ (mm) | $A_3$ (mm) | $A_4$ (mm) | $A_5$ (mm) | $A_6$ (mm) | $A_7$ (mm) | $A_8$ (mm) |
| Rectangular pulse | 19.708 | 18.834 | 17.382 | 15.358 | 12.780 | 9.672 | 6.084 | 2.168 |
| Meander-type pulse | 19.702 | 18.806 | 17.318 | 15.242 | 12.590 | 9.376 | 5.638 | 1.488 |
| $RD \cdot 100\%$ | 0.03 | 0.14 | 0.36 | 0.76 | 1.49 | 3.06 | 7.33 | 31.36 |
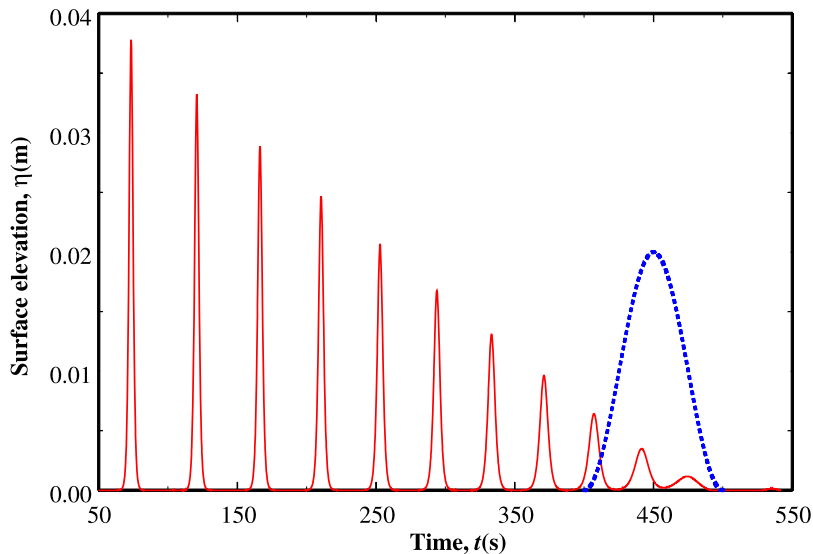


FIGURE 7. Cosine initial pulse (*dashed line*) and the result of its evolution at the distance $x = 6 \cdot 10^4 \, \text{m}$ (*solid line*).

part of the soliton spectrum (a right wing of soliton distribution function at large amplitudes) is described fairly good while at small amplitudes the distribution function may be not quite correct.

## 2.3. Cosine initial pulse

Let us now consider why the number of solitons emerging in each period of a pure periodic perturbation (as well as their amplitudes) differs from those emerging from the pulse-type perturbations of the same shape, amplitude and duration (*cf.* Fig. 2 with Figs. 3 and 4)? The answer is, apparently, as follows: In the pure periodic case the zero level of the physical system is not determined clearly. The system admits *the minimum of the wave field* as the zero level. Hence, a periodic sinusoidal perturbation can be treated as a periodic sequence of positive cosine-type pulses with respect to the minimum possible level. In a process of evolution, each pulse disintegrates into a number of solitons whose total amount is much greater than for sine-type perturbations considered above. New numerical simulation was carried out with this modified zero level for single cosine-type pulse as the initial perturbation; the result is shown in Figure 7.

There were clearly detected 11 solitons whose amplitudes are presented in Table 3. The amplitudes of solitons emerging from the periodic sinusoidal perturbation described above (see Sect. 2.1.1) are also shown in the same table for the comparison. This time soliton amplitudes for the sinusoidal perturbation were calculated more thoroughly using trace method suggested in [24]. When the sinusoidal perturbation disintegrates for the first time into the sequence of solitons ordered by their amplitudes as shown in Figure 2, the observer cannot see all

TABLE 3. Amplitudes of solitons, $A_k$, emerging from the cosine initial pulse and from the periodic sinusoidal perturbation.

| Initial pert. | $A_k$ | | | | | | | | | | |
|---|---|---|---|---|---|---|---|---|---|---|---|
| | $A_1$ (mm) | $A_2$ (mm) | $A_3$ (mm) | $A_4$ (mm) | $A_5$ (mm) | $A_6$ (mm) | $A_7$ (mm) | $A_8$ (mm) | $A_9$ (mm) | $A_{10}$ (mm) | $A_{11}$ (mm) |
| Cos., pulse | 37.75 | 33.25 | 28.89 | 24.68 | 20.63 | 16.77 | 13.09 | 9.636 | 6.422 | 3.49 | 1.15 |
| Sin., periodic | 33.70 | 30.39 | 26.92 | 23.36 | 19.60 | 15.54 | 11.43 | 8.04 | 5.66 | – | – |
| $RD \cdot 100\%$ | 10.73 | 8.60 | 6.82 | 5.35 | 4.98 | 7.35 | 12.65 | 16.60 | 11.82 | – | – |

solitons because some of them are still obscured. We followed up for the development of the wave field after the distance $x = 1.1 \cdot 10^4$ m which corresponds to Figure 2 and discovered that in the process of soliton interactions some more solitons of small amplitudes appear. So that the total number of solitons in this case was exactly the same as for the cosine initial pulse, $N = 11$. Their amplitudes were measured with respect to the minima of the initial sinusoidal perturbation. As one can see, the relative difference in percents between the corresponding soliton amplitudes for the cosine initial pulse and periodic sinusoidal perturbation, $RD = (A_k^c - A_k^s)/A_k^c$ is not too big now and not exceeds 17%. (see the last row of Tab. 3).

Thus, if the zero level of the considered physical system is known and the perturbation eventually vanishes at the infinity then the statistics of obscured solitons is determined by positive humps of the perturbation with respect to this zero level. Namely such a situation takes place in the case of hydrophysical measurements in laboratory (water tanks) or in natural marine conditions. But if the perturbation is periodic in principle, then solitons, their numbers and amplitudes are determined by each hump of the perturbation with respect to the total minimum of the initial perturbation.

## 2.4. Data processing: a model example

### 2.4.1. A model spectrum and the range of its validity

Let us apply now the developed approach to the random perturbation artificially generated and presented in Figure 1. This perturbation was obtained by means of inverse Fourier transform of a series of 128 harmonics having random phases in the interval $[0, 2\pi]$ and amplitudes distributed in accordance with the formula

$$S(\omega) = S_0(\omega + \omega_0)^{-2} \tanh \frac{\omega}{\delta\omega}, \tag{2.27}$$

where $S_0 = 2 \cdot 10^{-4}$ m, $\omega_0 = 2\pi \cdot 10^{-2}$ s$^{-1}$, and $\delta\omega = 2.5 \cdot 10^{-2}$ s$^{-1}$.

For the construction of quasi-random wave field it was taken only the low-frequency and most energetic part of this spectrum, $0 \le \omega \le \omega_{lim}$, where $\omega_{lim} = 0.767$ s$^{-1}$ (see vertical dashed line in Fig. 8). The limiting frequency, $\omega_{lim}$, was chosen for the following reasons. The dispersion relation for infinitesimal perturbations within the TKdV equation (2.1) is

$$k = \frac{\omega}{c_0} + \frac{h^2}{6c_0^3}\omega^3 = \frac{\omega}{c_0}\left(1 + \frac{h^2}{6c_0^2}\omega^2\right), \tag{2.28}$$

where $\omega$ is the frequency of a sinusoidal wave, and $k$ is the wave number, $\eta \sim e^{i(\omega t - kx)}$.

As is well known, this dispersion relation represents an approximation of a real dispersion relation of a physical system, *e.g.*, water or plasma waves, when $\omega, k \to 0$. The range of validity of the dispersion relation (2.28) is restricted by the requirement that the second term in brackets is small in comparison with one (see,
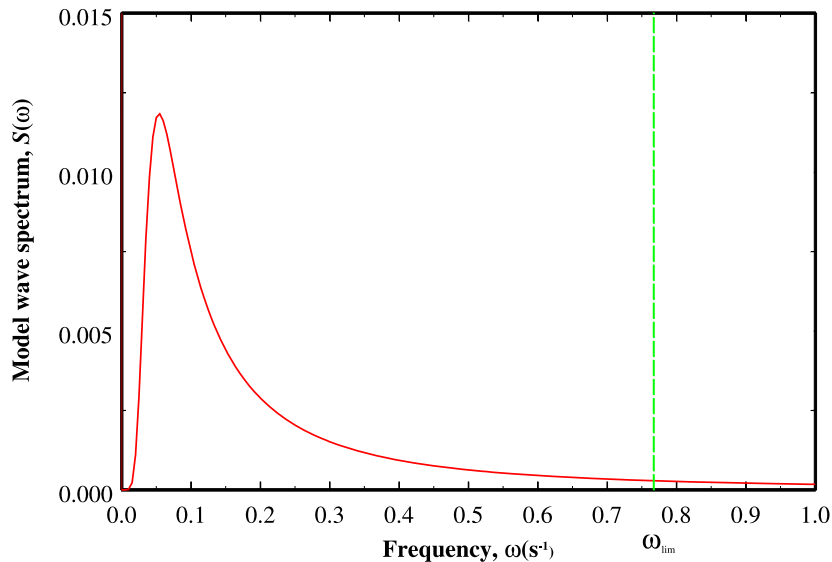
FIGURE 8. The model amplitude spectrum of random wave field shown in Figure 1.

*e.g.*, [1, 15, 29]). This condition gives

$$\omega \ll \omega_{cr} \equiv \frac{c_0}{h}\sqrt{6} = \sqrt{\frac{6g}{h}}. \qquad (2.29)$$

In our case $\omega_{cr} \approx 7.67\,\text{s}^{-1}$. To satisfy condition (2.29), we set $\omega_{lim} = 0.1\omega_{cr} = 0.767\,\text{s}^{-1}$.

### 2.4.2. Data processing of the model initial perturbation

Let us consider now a quasi-random wave field shown in Figure 1 and apply the approach developed above. Each positive hump enumerated in the figure can be studied separately by means of the numerical code for the TKdV equation (2.1). The numerical code was based on the explicit finite-difference scheme of a second-order accuracy both on spatial and temporal variables [2]. The theoretical analysis shows that used central-difference scheme is conditionally stable provided that $\Delta x \sim \Delta t^3$, where $\Delta x$ and $\Delta t$ are the spatial and temporal mesh steps. The code works very effectively and fast so that the result of pulse fission on solitons was obtained very quickly. A typical picture of disintegration of one of the pulses (pulse No. 5 in Fig. 1) is shown in Figure 9.

The number of emerged solitons and their parameters can be easily calculated. To avoid errors in determination of soliton parameters, the numerical calculations were conducted until each soliton was sufficiently separated from others, so that their fields were not overlapped in the vicinity of their maxima. This procedure was carried out for each pulse shown in Figure 1. As the result, it was obtained a large number of solitons of different amplitudes, their total number for all pulses was $N_s = 73$ which is enough for the illustrative purposes. The solitons were collected into several groups (15 groups in total) according to their amplitudes. This allowed us to construct a histogram of numbers of solitons *versus* their amplitudes. The histogram can be considered as a model of the distribution function $f(A)$ of density of number of solitons on amplitudes (see Eq. (2.9)). The histogram obtained and the model distribution function for the considered illustrative example are shown in Figure 10. Frame (b) in the figure shows the cumulative distribution function, *i.e.*, the total number of solitons whose amplitudes are not greater than the given value.
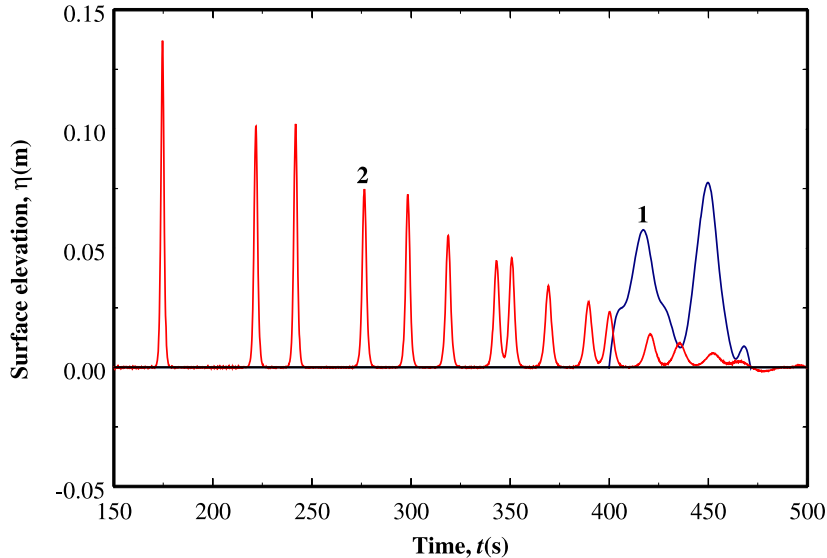
FIGURE 9. Disintegration of one of the initial random pulses (line 1) on solitons (line 2).

## 3. LABORATORY EXPERIMENT WITH WIND WAVES ON SHALLOW WATER

The theory developed above was applied to the data of laboratory experiments with wind wave generation. Series of experiments were carried out in the Luminy (Marseilles) small tank made of plexiglass and having the following sizes (length × width × height): 865 cm × 64 cm × 50 cm. The water depth in the tank in different experiments ranged from 1 cm to 8 cm: $h = 1, 2, 3, 4, 6$ and 8 cm. Surface waves were generated by a wind blowing up over the water surface with the different mean velocities: $V_w = 5.29, 6.45, 8.62$ and 13.24 m/s. The ventilator producing an air flow was installed at one of the ends of the tank. The blower width was the same as the width of the tank, 64 cm, but its height was 31 cm above the water level. The tank was covered above the blower by a plexiglass lid. At the opposite end of the tank it was placed a wave absorber to exclude reflected waves (an inclined bottom causing surface wave breaking). Two sensitive electric probes recording water level were placed at the distances 100 cm and 300 cm from the ventilator. The probes were thoroughly calibrated before each experiment; their sensitivities were equal and amounted $s = 0.61$ V/cm.

Below we present the analysis of only one of the series of experiments with the water depth $h = 1$ cm and wind velocity $V_w = 5.29$ m/s. Other experimental series were analysed in a similar way. We have to make a reservation in advance that the experimental data with wind waves are not perfect for the illustration of suggested approach. Wind waves generated by permanently blowing wind is an active system, *i.e.*, the system with the permanent energy pumping at each point of water surface. Moreover, a distributed external force due to wind is not a constant, it varies from some maximum value near the ventilator to some small value at the opposite end of the tank. This results in the different soliton distribution functions measured at two different distances from the ventilator. A small water viscosity can also affect the soliton distribution function.

Another difficulty with surface waves generated by wind is the effective generation of high frequency Fourier components, so that the essential portion of wave energy is contained in that part of Fourier spectrum which is beyond the range of validity of KdV equation. Therefore we were forced to restrict our analysis by only the low-frequency components of the wave spectrum. Figure 11 presents the Fourier spectrum of wind waves recorded at two distances from the ventilator as indicated above. The critical frequency at $h = 1$ cm is $\omega_{cr} = 76.7\,\mathrm{s}^{-1}$, and to satisfy the condition (2.29) we cut the Fourier spectra of wind waves at $\omega_{lim} = 13.4\,\mathrm{s}^{-1}$ (see dashed vertical line in Fig. 11) and ignored the high frequency portions of spectra above $\omega_{lim}$.
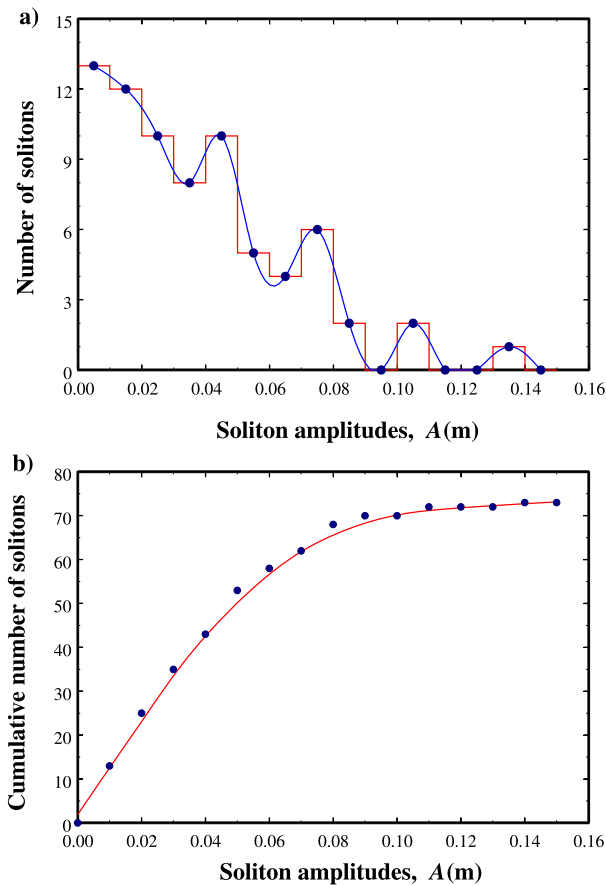
FIGURE 10. Frame (a) – the histogram of soliton distribution (*piece-linear line*) and the model distribution function (*smooth line*) for the illustrative example. Frame (b) – the cumulative distribution function *versus* soliton amplitude corresponding to the model distribution function shown in frame (a). Smooth lines in both frames were obtained by means of spline interpolation of numerical data.

The surface perturbation was reconstructed by means of the inverse Fourier transform on the basis of extracted portions of wave spectra in the range $0 < \omega \le \omega_{lim}$). The fragments of 60-second duration records corresponding to two spatial points of measurements are shown in Figure 12.

As it is clearly seen from the comparison of two data records presented in frames (a) and (b), there is the essential difference between them, especially in the intensity of wave fields. This can be explained by the effect of a fetch on wind wave generation. Therefore, one can expect that the statistics of obscured solitons in the record of frame (b) is essentially richer than in frame (a).

The recorded data shown in Figure 12 were used as the input data for the TKdV equation (2.1). In the statistically equilibrium state each 60 s portion of recorded data is equivalent to the same portion taken at a different time, therefore one can expect that the number of solitons obscured in each portion of data is the same in average and their distribution function is invariant with respect to time shift. This was confirmed in the data processing.

The TKdV equation (2.1) was solved numerically using the recorded data of 60 s duration from the total time interval of 208 s. After a while solitons emerged from the quasi-random data, and their amplitudes were easily determined with the help of a special subroutine. This allowed us to determine the histogram of soliton numbers
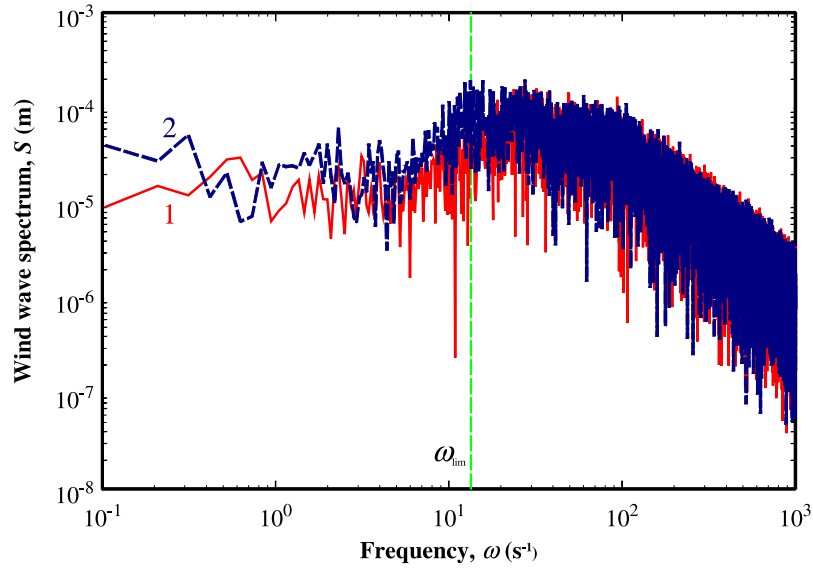
FIGURE 11. Fourier spectrum of wind waves generated in the laboratory tank at two different distances from the ventilator. Solid line 1 represents the spectrum at the distance 100 cm; dashed line 2 represents the spectrum at the distance 300 cm.
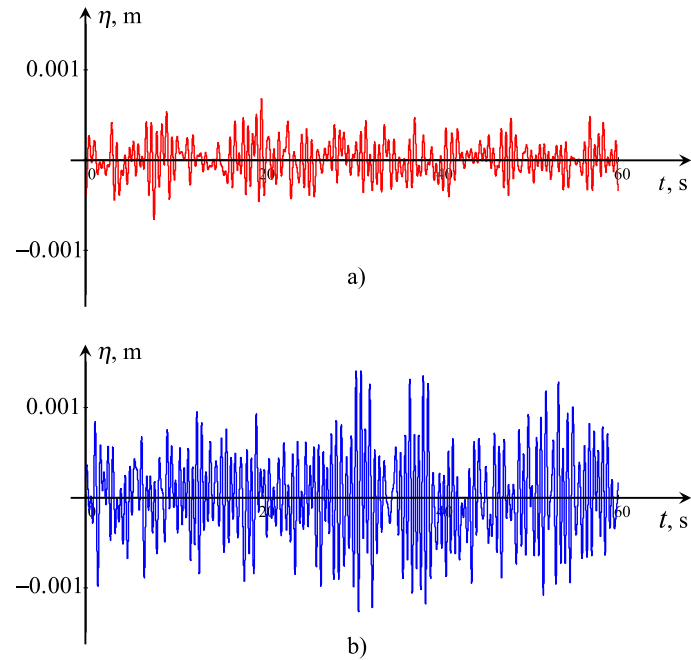


FIGURE 12. Fragments of low-frequency components of surface perturbations generated by wind in two spatial points of measurements in the tank. Frame (a) – surface perturbation at the distance 100 cm; frame (b) – at the distance 300 cm.
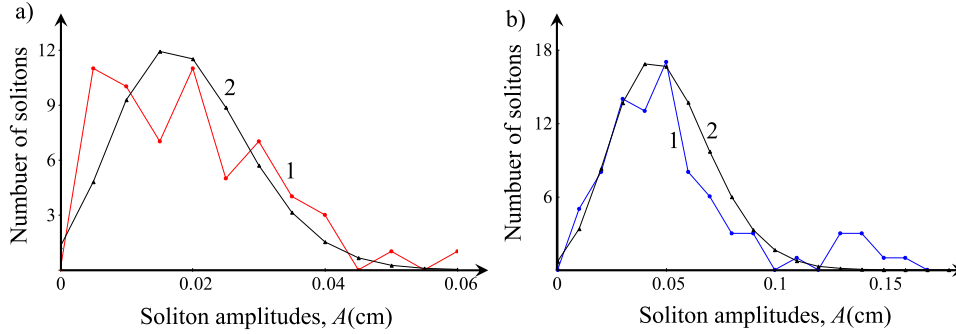
FIGURE 13. The histogram of soliton numbers *versus* soliton amplitudes for the time series shown in Figure 12. Line 1 in each frame represent experimental data, and lines 2 – the best fit of these data by the Poisson distribution functions with the parameters $\lambda = 3.85$ for the histogram shown in frame (a) and $\lambda = 4.94$ for the histogram shown in frame (b).
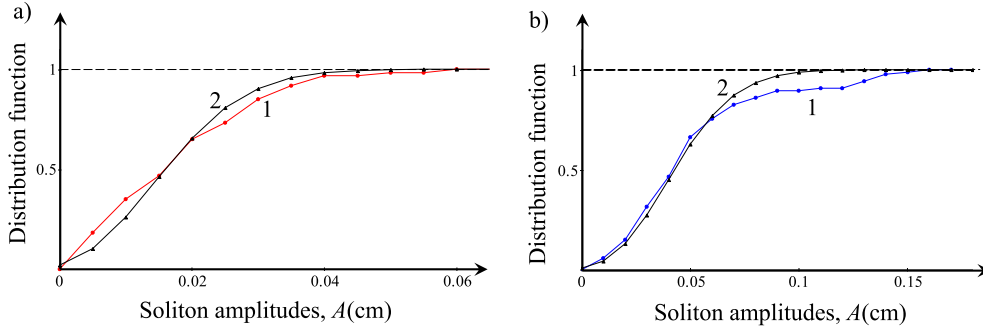


FIGURE 14. The integral (cumulative) distribution functions (lines) for the experimental data shown in Figure 12. Lines 2 represent the best fit approximation with the Poisson cumulative distribution functions with the same parameters $\lambda$ as in Figure 13.

in the each particular interval of amplitudes $A + \Delta A$; this is the analog of a differential distribution function. On the basis of this function we determined also the integral (cumulative) distribution function – the total number of solitons with the amplitudes less than $A$ normalised by the total number of all solitons. Figure 13 demonstrates the histogram of soliton numbers *versus* amplitudes for the time series shown in Figure 12. The experimental data can be approximated by the Poisson distribution function $P(n) = \lambda^n e^{-\lambda}/n!$, where the parameter $\lambda = 3.85$ for the histogram shown in frame (a) and $\lambda = 4.94$ for the histogram shown in frame (b).

The corresponding integral distribution functions for the experimental data of Figure 12 are shown in Figure 14 (lines 1) together with the approximative Poisson integral functions with the same parameters as in Figure 13. The total number of solitons emerged from the wave field shown in Figure 12a was 60, and emerged from the wave field shown in Figure 12b was 86. As expected, the time series recorded closer to the ventilator (Fig. 12a) contained less number of solitons than the time series recorded further from the ventilator (Fig. 12b). In the latter case the wave field was much better developed due to the influence of wave fetch.

If we assume that all 60 solitons in the time series shown if Figure 13a are uniformly distributed in the time interval of 60 s, then we obtain that the time interval per each soliton is $\Delta T_1 = 1$ s. As follows from the histogram shown in Figure 13a the maximal number of solitons have amplitudes $A_{m1} = 0.02$ cm and the duration $T_{s1} = 0.026$ s. Therefore $\Delta T_1/T_{s1} \approx 3.85$. The similar estimates for the time series shown if Figure 13b give the time interval per each soliton $\Delta T_2 \approx 0.7$ s. As follows from the histogram shown in Figure 13b the maximal number of solitons in this time series have amplitudes $A_{m2} = 0.05$ cm and the duration $T_{s2} = 0.165$ s. Therefore
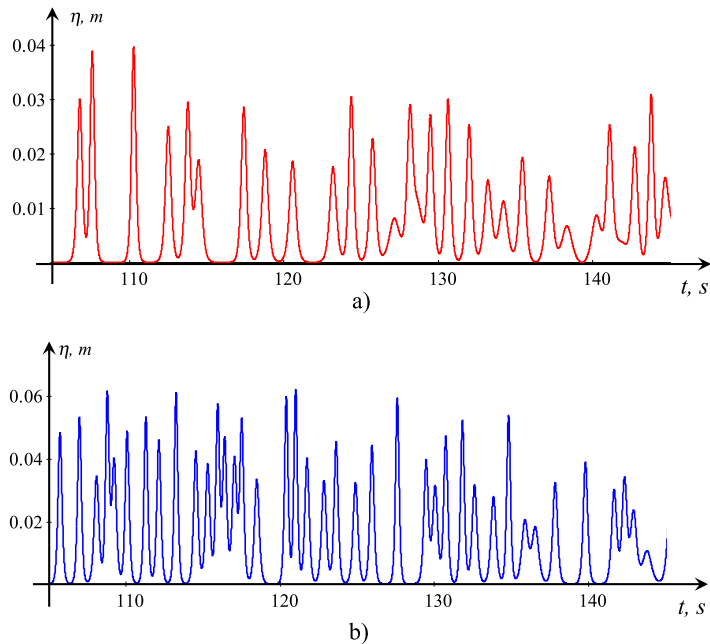
FIGURE 15. The fragments of numerical calculations with the input data taken from Figure 12 illustrating the soliton gas density in both time series.

$\Delta T_2/T_{s2} \approx 4.2$. Thus, we see that in both cases the "soliton gas" is very dense (*cf.* [8, 28]). The fragments of numerical calculations presented in Figure 15 illustrate the soliton gas density in both time series.

## 4. CONCLUSION

To analyze long random time series of water waves in shallow basins we have proposed an approach which differs from the traditionally used Fourier analysis. Our approach is based on the extraction of obscured solitons from the complex wave fields and construction of histograms of solitons at different points of observation. The histograms can be considered as experimental counterpart of distribution functions of number of solitons on their amplitudes. According to the theoretical conception, a soliton component of a wave field in the well-developed nonlinear perturbations should dominate. As is well known, the number and individual parameters of solitons preserve in the conservative statistically homogeneous systems [30, 31], therefore the distribution function (or histograms of solitons) is the same at different points of observation if the dissipative factors (*i.e.*, viscosity or external sources of energy) are negligible. In contrast to that the Fourier spectrum changes due to nonlinearity.

Our approach is in line with the contemporary development of the theory of strong turbulence in the integrable or near-integrable systems [3, 5–9, 28, 31]. Experimentally constructed distribution function can be used for the determination of degree of soliton gas density – how far the density is from the critical value as defined in references [8, 28]. Data processing of laboratory experiments presented in our paper supplement the data processing of field experiments reported in reference [5].

A small dissipation can cause a gradual decay of soliton histograms and their distortion, in general. The histogram decay and its distortion depend on the specific type of dissipation; this problem has not been studied yet, although the decay of individual solitons under the influence of various types of dissipation has been investigated for the KdV [12] and Benjamin–Ono [13] solitons, as well as for the Kadomtsev–Petviashvili lumps [4].

Our approach can provide some additional valuable information about the energy distribution in natural wave fields such as the relationship between the soliton and nonsoliton components of the perturbation, and may indicate on the existence and intensity of external sources or sinks of energy.

To determine the soliton number and amplitudes from the random time series, we applied direct numerical modelling for the evolution of initial data within the framework of the TKdV equation (2.1). The existing numerical codes (see, *e.g.*, [2]) allow us to obtain the results fairly quickly in the form convenient to further analysis. However, it is not the only method which can be applied; the numerical solution of the eigenvalue problem (2.22) can also be convenient and useful. Our experience with the application of the approach developed here shows that there is no problem with the determination of number and amplitudes of intense solitons, *i.e.*, solitons of big and moderate amplitudes. However, it takes more efforts to determine parameters of solitons whose amplitudes are very small. In general, an uncertainty in the determination of parameters of solitons of very small amplitudes is higher than of moderate and big solitons. Meanwhile, the model example of Section 2.4.2 shown in Figure 10, as well as the experimental laboratory data shown in Figure 13 demonstarte that the number of such small-amplitude solitons may be relatively big.

As has been mentioned, the soliton distribution function remains unchanged in the integrable systems. However, the wave field randomly fluctuates in the process of evolution. This leads to the random fluctuations of local wave extrema. As has been shown in reference [28], the distribution function of wave extrema varies with time even when the wave field consists of solitons only. This can be of interest from the viewpoint of physical applications, but beyond the scope of this paper.

In conclusion, we emphasize that the approach developed here is applicable to the KdV-type systems, *e.g.*, shallow-water waves (see, for example, Ref. [6] where the turbulence of soliton gas was studied both within the integrable KdV and non-integrable KdV-BBM equations). Its generalization to deep-water waves described by the Benjamin–Ono or nonlinear Shrödinger equation is the interesting and challenging problem.

## References

[1] M.J. Ablowitz and H. Segur, Solitons and the Inverse Scattering Transform. SIAM, Philadelphia (1981).

[2] Yu. Berezin, Modelling Nonlinear Wave Processes. VNU Science Press (1987).

[3] F. Carbone, D. Dutykh and G.A. El, Macroscopic dynamics of incoherent soliton ensembles: soliton gas kinetics and direct numerical modelling. *Eur. Phys. Lett.* **113** (2016) 30003.

[4] S. Clarke, K. Gorshkov, R. Grimshaw and Y. Stepanyants, Decay of Kadomtsev-Petviashvili lumps in dissipative media. *Physica D* **366** (2018) 43–50.

[5] A. Costa, A.R. Osborne, D.T. Resio, S. Alessio, E. Chrivi, E. Saggese, *et al.* Soliton turbulence in shallow water ocean surface waves. *Phys. Rev. Lett.* **113** (2014) 108501.

[6] D. Dytukh and E. Pelinovsky, Numerical simulation of a solitonic gas in KdV and KdV-BBM equations. *Phys. Lett. A* **378** (2014) 3102–3110.

[7] A.G. El, The thermodynamic limit of the Whitham equations. *Phys. Lett. A* **311** (2003) 374–383.

[8] G.A. El, Critical density of a soliton gas. *Chaos* **26** (2016) 023105.

[9] G.A. El and A.M. Kamchatnov, Kinetic equation for a dense soliton gas. *Phys. Rev. Lett.* **95** (2005) 204101.

[10] S. Flügge, Practical Quantum Mechanics. Springer-Verlag, Berlin (1971).

[11] J.-P. Giovanangeli, C. Kharif, N. Raj, Y. Stepanyants, Nonlinear spectra of shallow water waves, in *Conf. Proc., OCEANS'13 MTS/IEEE San Diego, USA, paper number 130503-040* (2013).

[12] R. Grimshaw, E. Pelinovsky and T. Talipova, Damping of large-amplitude solitary waves. *Wave Motion* **37** (2003) 351–364.

[13] R. Grimshaw, N. Smyth and Y. Stepanyants, Decay of Benjamin–Ono solitons under the influence of dissipation. *Wave Motion* **78** (2018) 98–115.

[14] V.M. Kamenkovich and A.S. Monin (eds.), Okeanologia. Nauka, Moscow Vols. 1, 2 (in Russian) (1978).

[15] V.I. Karpman, Nonlinear Waves in Dispersive Media. Nauka, Moscow (1973) (in Russian) Engl. transl.: Pergamon Press, Oxford, (1975).

[16] O. Kurkina, E. Rouvinskaya, T. Talipova, A. Kurkin and E. Pelinovsky, Nonlinear disintegration of sine wave in the framework of the Gardner equation. *Physica D* **333** (2016) 222–234.

[17] O. Kurkina, E. Rouvinskaya, A. Giniyatullin, A. Kurkin, T. Talipova and E. Pelinovsky, Long sine wave transformation in the framework of Gardner equation: spectral and statistical analysis. *Int. J. Math. Models Methods Appl. Sci.* **10** (2016) 381–387.

[18] L.D. Landau and E.M. Lifshitz, Quantum Mechanics – Nonrelativistic Theory, 4th edn. Nauka, Moscow (1989) (in Russian). (Engl. transl.: 3rd edition Pergamon Press, Oxford, 1981).

[19] A.P. Nagovitsyn, E.N. Pelinovsky and Yu.A. Stepanyants, Observation and analysis of solitary internal waves in the coastal zone of the Sea of Okhotsk. (English translation of the Russian journal Morskoi Gidrofizicheskii Zhurnal) *Sov. J. Phys. Oceanogr.* **2** (1991) 65–70.

[20] A.R. Osborne, The inverse scattering transform: tools for the nonlinear Fourier analysis and filtering of ocean surface waves. *Chaos Solitons Fractals* **5** (1995) 2623–2637.

[21] A.R. Osborne, Solitons in the periodic Korteweg–de Vries equation, the $\Theta$-function representation, and the analysis of nonlinear, stochastic wave trains. *Phys. Rev. E* **52** (1995) 1105–1122.

[22] A.R. Osborne, Nonlinear Ocean Waves and the Inverse Scattering Transform. Academic Press, Boston (2010).

[23] A.R. Osborne, E. Segre, G. Boffetta and L. Cavaleri, Soliton basis states in shallow-water ocean surface waves. *Phys. Rev. Lett.* **67** (1991) 592–595.

[24] A. Salupere, G.A. Maugin and J. Engelbrecht, Korteweg–de Vries soliton detection from a harmonic input. *Phys. Lett. A* **192** (1994) 5–8.

[25] A. Salupere, P. Peterson and J. Engelbrecht, Long-time behaviour of soliton ensembles, part I – emergence of ensembles. *Chaos Solitons Fractals* **14** (2002) 1413–1424.

[26] A. Salupere, P. Peterson and J. Engelbrecht, Long-time behaviour of soliton ensembles, part II – periodical patterns of trajectories. *Chaos Solitons Fractals* **15** (2003) 29–40.

[27] E. Segre, G. Boffetta, A.R. Osborne and M. Petti, Analysis of laboratory surface wave data using the scattering transform for the periodic Korteweg–de Vries. *Chaos Solitons Fractals* **8** (1995) 1935–1943.

[28] E.G. Shurgalina and E.N. Pelinovsky, Dynamics of irregular wave ensembles in the coastal zone. Nizhny Novgorod State Technical University, Nizhny Novgorod (2015).

[29] G.B. Whitham, Linear and Nonlinear Waves. Wiley – Interscience, New York (1974).

[30] V.E. Zakharov, Kinetic equation for solitons. *Sov. Phys. JETP* **33** (1971) 538–541.

[31] V.E. Zakharov, Turbulence in integrable systems. *Stud. Appl. Math.* **122** (2009) 219–234.